INSTITUTE OF PHYSICS PUBLISHING NONLINEARITY

Nonlinearity **16** (2003) C1–C10 PII: S0951-7715(03)55992-8

COVER ILLUSTRATION

Pattern formation in vertically oscillated convection

Jeffrey L Rogers[1,3], **Werner Pesch**[2] **and Michael F Schatz**[3]

[1] HRL Laboratories LLC, Malibu, CA 90265, USA
[2] Physikalisches Institut der Universität Bayreuth, 95447 Bayreuth, Germany
[3] Center for Nonlinear Science and School of Physics, Georgia Institute of Technology, Atlanta, GA 30332-0430, USA

Received 12 November 2002
Published 9 December 2002
Online at stacks.iop.org/Non/16/C1

Abstract

A fluid layer driven out of equilibrium by both a thermal gradient and time-periodic vertical oscillations displays a number of interesting behaviour. Here we review results from the first experimental investigation of this system as well as a number of related and novel numerical findings. At primary onset these results include modulation-enhanced conduction stability as well as fluid motion in either harmonic or subharmonic resonance with the drive frequency. In the nonlinear parameter range we find a wide variety of singly resonant states, a region where both temporal responses coexist, and a number of novel coexistence patterns–including quasiperiodic crystals and superlattices. Four-wave interactions between harmonic and subharmonic modes are shown to select the structure of these complex patterns. The role of inversion symmetry in the emerging planforms is discussed.

M This article features multimedia enhancements available from the abstract page in the online journal; see `www.iop.org`.

1. Background

Two of the most commonly studied examples of nonequilibrium pattern forming systems are drawn from hydrodynamics: a fluid layer with an imposed vertical temperature difference (Rayleigh–Bénard convection [1, 2]) and an open dish of vertically oscillated fluid (Faraday surface waves [3]). These systems have substantial differences, for example, the basic pattern formation mechanisms, as well as important similarities, including the role of symmetry in selecting the planform near onset. Many of the characteristics that are distinctive to patterns in either Rayleigh–Bénard convection or Faraday surface waves can be found in a single system: a fluid layer driven by both a vertical temperature difference and sinusoidal vertical oscillations (figure 1). This paper is intended to give the reader an introduction to pattern formation in vertically oscillated convection. More detailed treatment of the topics reviewed here may be found in the cited references.

One important distinction between Rayleigh–Bénard convection and Faraday surface waves is the mechanism which selects a pattern's lengthscale. At onset in a Rayleigh–Bénard

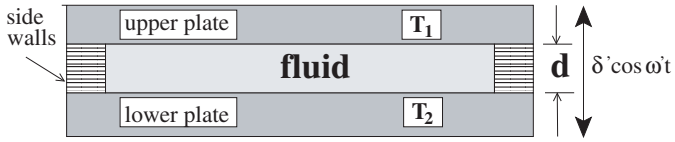

Figure 1. Fluid motion in the layer of depth d is driven both by the imposed temperature difference $\Delta T = T_2 - T_1$ and the vertical oscillations $\delta' \cos \omega' t$. In addition to the Rayleigh–Bénard convection parameters of Pr and R, this system is characterized by two nondimensional modulation parameters δFr and ω (see text).

apparatus the emerging buoyancy driven pattern is stationary with a wavenumber $q = q_c$ determined by geometric constraints [4]. In particular, q_c is directly proportional to the inverse of the fluid layer depth d (figure 1). In contrast, persistently time-dependent Faraday surface waves are driven by vertical oscillations, often sinusoidal, with a drive period τ. This time-dependent driving is a form of parametric modulation and leads to wavenumber selection by the forcing frequency, which is related to the dispersion relation of the waves.

Communality between the two systems is reflected in the role of pattern symmetries near onset. In this parameter region the behaviour of exponentially growing linear modes is captured by equations for the spectral mode amplitudes A, whose terms must satisfy spatial and temporal symmetries. These constraints are important since nonlinear terms in these equations correspond to the competition and interactions between emerging modes and, thus, dictate the pattern planform. When the approximation of inversion symmetry is valid, amplitude equations are invariant under the inversion $A \to -A$, causing even order terms to be excluded and thereby strongly influencing the pattern structure. Inversion symmetry in Rayleigh–Bénard convection takes the form of spatial invariance under vertical reflection about the fluid layer midplane (Boussinesq symmetry). If this symmetry is approximately present, stripe (convection roll) patterns are typically observed at onset, while in the absence of this symmetry hexagons form. In contrast, inversion symmetry in Faraday waves is temporal, namely, invariance under discrete time translation by τ and displayed in the subharmonic (periodic at 2τ) waves frequently observed near onset. Stimulating a harmonic response in the surface waves—by using thin layers, a viscoelastic fluid, or multiple oscillation frequencies—causes a breaking of this symmetry.

The majority of pattern formation studies in Rayleigh–Bénard convection, Faraday surface waves, as well as other nonequilibrium pattern forming systems have focused on the cases when a single q is accessible at onset [2]. By allowing for multiple and distinct accessible wavenumbers near onset, recent investigations have extended this focus and, in the process, found a number of exotic patterns including quasiperiodic crystals, superlattices, and domain coexistence [5]. Many of these patterns display complex spatial structures, often on distinct lengthscales, described by relatively few spectral modes. Due to these characteristics, Pismen [6] has designated such patterns as *complex order*. Classification of these states can be refined to quasiperiodic crystals and superlattices using criteria given by Lifshitz [7]. The essential difference between quasiperiodic crystals and superlattices is the number of basic (indexing) vectors required to map out the dominant spectral modes. If the number of indexing vectors is greater than the spatial dimension of the pattern (two in the present case), then the complex state is a quasiperiodic crystal. A superlattice exists when the number of indexing vectors equals the pattern's spatial dimension. Quasiperiodic crystals and superlattices have been reported in other hydrodynamic [8–13] and optical systems [5, 14, 15] where quasiperiodic crystals have been termed quasipatterns and quasicrystals. The majority of these studies involve Faraday surface waves where degeneracy of the dispersion relation translates into two distinct classes (harmonic and subharmonic) of wavenumbers that can be simultaneously excited. In most

cases three-wave spectral mode resonances (*resonant triads*) are the formation mechanism for complex-ordered patterns. We will show that complex order also forms in vertically oscillated convection; however, in this system such patterns arise from four-wave resonances (*resonant tetrads*). Moreover, the mathematical description of these patterns is free of the approximations required for Faraday systems. Vertically oscillated convection also permits easy selection of different interacting lengthscales from a range of wavenumbers, thereby allowing flexibility in the spectral resonances which form.

Vertically oscillated convection is described by four nondimensional parameters: two from Rayleigh–Bénard convection and two from parametrically driven systems. A Rayleigh–Bénard convection experiment (no vertical oscillations) of infinite lateral extent is described by the Boussinesq equations which contain two nondimensional parameters: Rayleigh number R and Prandtl number Pr. These are defined,

$$R = \frac{\alpha g d^3 \Delta T}{\nu \kappa} \qquad \text{and} \qquad Pr = \frac{\nu}{\kappa}, \tag{1}$$

in terms of ΔT (figure 1), gravitational acceleration g, d, thermal diffusivity κ, kinematic viscosity ν, and thermal expansivity α. In Rayleigh–Bénard convection R characterizes the strength of the thermally induced buoyancy forces driving the fluid system away from equilibrium. Intrinsic scales in the system are d and the vertical diffusion time ($t_v = \kappa/d^2$). In our compressed gas convection experiments, $d \approx 0.6$ mm and $t_v \approx 1.6$ s. Imposing vertical oscillations of the form $\delta' \sin \omega' t$ on Rayleigh–Bénard convection [16, 17] simply adds a time-periodic term to the gravity constant in the Boussinesq equations, requiring two additional nondimensional (modulation) parameters to describe the complete driving in the system. These are the displacement amplitude δFr and modulation frequency ω:

$$\delta Fr = \frac{\kappa^2}{d^4 g}\delta' \qquad \text{and} \qquad \omega = \frac{d^2}{\kappa}\omega', \tag{2}$$

where δ' is the dimensional displacement amplitude and ω' is the dimensional angular frequency of oscillation. It is important to note that unlike the Faraday wave system, there is no free surface in our studies of vertically oscillated convection; the time-dependent acceleration in our system couples to temperature-induced density differences in the flow. The experimental devices and numerical methods used in this investigation have been described elsewhere [18–20].

2. Primary onset and singly resonant patterns

In the current system the uniform conduction state competes with temporally modulated convection over a wide range of parameter values. Our studies focus on this competition for the case of fixed Pr and ω. By varying the remaining control parameters δFr and R over a range where R is not too large, conduction is found to lose stability to flows with either a harmonic or subharmonic temporal response. Intuitively, vertically oscillated convection can be understood by analogy with an inverted pendulum mounted on a vertically oscillating base. The vertical oscillations are included as a time-periodic term in the gravity (parametric modulation). This analogy can be made more quantitative by an approximate mapping of the Boussinesq equations onto a Mathieu equation. Previous investigations of vertically oscillated convection have used this analogy [16], as well as numerical Galerkin methods [17], to perform linear stability analyses predicting that harmonic and subharmonic fluid motion occur at distinct spatial scales. Our own linear stability analysis is found to be in agreement with the previous work. Essential results from these analyses are that harmonic flows are more stable than unmodulated convection, i.e. the critical Rayleigh number R_c for harmonic convection (R_c^H) is expected to be larger than the R_c in the absence of modulation ($R_c^0 = 1708$).

In contrast, subharmonic flows may be either more stable ($R_c^S > R_c^0$) or less stable ($R_c^S < R_c^0$). For $R > 0$ the critical wavenumber of harmonic patterns q_c^H is significantly less than the critical wavenumber of subharmonic patterns q_c^S. Linear stability curves for harmonic and subharmonic onsets bisect at a bicritical point where both q^H and q^S are accessible. In previous papers we have confirmed these linear stability predictions with experiments for both R_c and q_c [21,22] at fixed $Pr = 0.930$ and $\omega = 98.0$ as well as the temporal responses [19] of both harmonic and subharmonic patterns.

Purely harmonic patterns occur when the parametric driving is relatively small, and they are qualitatively similar to states observed in Rayleigh–Bénard convection. Near primary onset, the observed pattern depends on both the validity of the Boussinesq symmetry and the magnitude of sidewall forcing. As long as ΔT is not large, the Boussinesq symmetry is valid and a striped state is found near onset. If the sidewalls result in relatively weak forcing parallel stripes (figure 2(*a*)) are the striped state. When the sidewall forcing is stronger

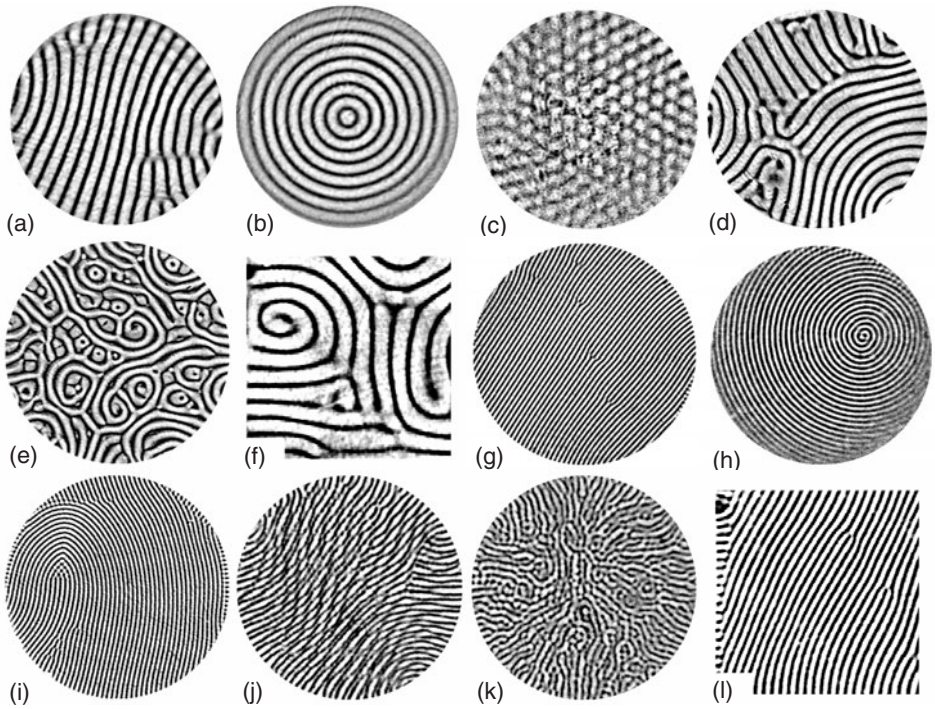

Figure 2. Representative purely harmonic ((*a*)–(*f*)) and purely subharmonic ((*g*)–(*l*)) patterns observed in experiments for $Pr = 0.93$, unless noted otherwise. Near harmonic onset (*a*) parallel stripes ($R = 4529$, $\delta Fr = 3.49 \times 10^{-4}$, and $\omega = 98.0$), (*b*) targets ($Pr = 0.924$, $R = 4050$, $\delta Fr = 3.59 \times 10^{-4}$, and $\omega = 98.5$), and (*c*) hexagons ($R = 4858$, $\delta Fr = 3.62 \times 10^{-4}$, and $\omega = 98.1$) occur. Away from onset parallel stripes (*d*) display defects ($R = 3926$, $\delta Fr = 3.36 \times 10^{-4}$, and $\omega = 98.4$) and sufficiently into the harmonic convective region (*e*) spiral defect chaos ($R = 4384$, $\delta Fr = 2.59 \times 10^{-4}$, and $\omega = 96.2$) forms. Similar states (*f*) are observed with square sidewalls ($Pr = 0.893$, $R = 5025$, $\delta Fr = 3.17 \times 10^{-4}$, and $\omega = 99.7$). Near subharmonic primary onset (*g*) parallel stripes ($R = 4857$, $\delta Fr = 3.74 \times 10^{-4}$, and $\omega = 97.9$), (*h*) giant spirals ($R = 4108$, $\delta Fr = 4.12 \times 10^{-4}$, and $\omega = 97.9$), and (*i*) giant convex disclinations ($R = 4385$, $\delta Fr = 4.31 \times 10^{-4}$, and $\omega = 96.2$) are found. Away from onset (*j*) transverse modulated stripes ($R = 6128$, $\delta Fr = 4.33 \times 10^{-4}$, and $\omega = 95.0$) and (*k*) radial stripes ($R = 6639$, $\delta Fr = 4.31 \times 10^{-4}$, and $\omega = 95.1$) are common. Similar results are observed with (*l*) square sidewalls ($Pr = 0.894$, $R = 5037$, $\delta Fr = 4.40 \times 10^{-4}$, and $\omega = 99.8$).

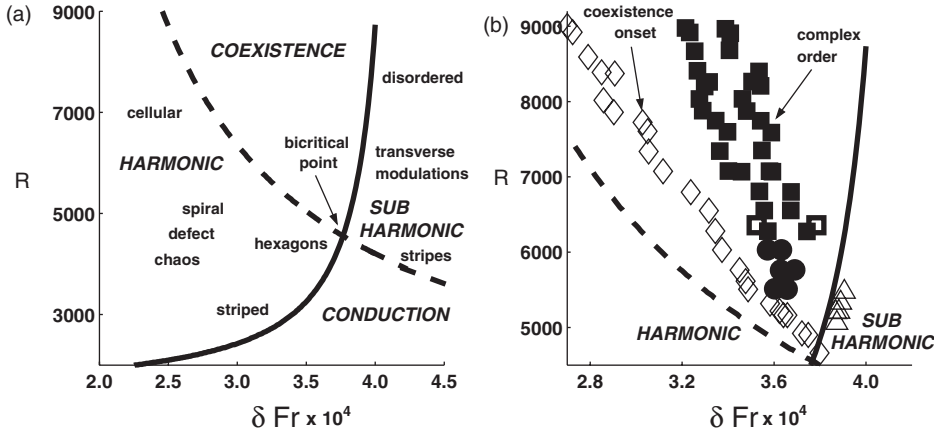

Figure 3. Slices of parameter space for fixed $Pr = 0.930$ and $\omega = 98.0$. Part (a) shows general pattern regions observed in experiments while (b) focuses on the coexistence region. Linear stability predictions for the onset of temporal modulated flows from the conduction state are shown: (——) harmonic and (- - - -) subharmonic. Observed onsets of coexistence in experiments from pure harmonic (◇) and pure subharmonic patterns (△) are shown in (b). Boundaries for complex order determined in experiments (■) are in agreement with simulations for $R > 6280$; for comparison, boundaries found in simulations (□) are shown at $R \approx 6300$. Simulations find complex order extends down to the bicritical point [19, 24], while experiments find patterns (●) with mixed harmonic cellular symmetries (see [21, 22]).

targets form. Both light core (figure 2(b)) and dark core [22] targets are observed. If the Boussinesq symmetry is not valid, hexagons form at onset (figure 2(c)). Under the conditions of our experiments [19] hexagons are observed only in the vicinity of the bicritical point (figure 3(a)), where ΔT is several times larger than the onset value required in the absence of vertical oscillations.

Each type of harmonic onset planform (parallel stripes, targets, and hexagons) displays a different route to a common complicated state as the experiment moves away from onset and into the harmonic parameter region. While onset planforms are relatively regular, various kinds of irregularities or defects form as the system moves away from onset. Parallel stripes display dislocations and curvature about two sidewall foci (figure 2(a)). Continuing away from onset, the number of dislocations and the stripe curvature increase resulting in amplitude grain boundaries, as shown in figure 2(d), as well as additional sidewall foci. Sufficiently far from onset, spiral defect chaos (figure 2(e)) forms. In contrast, a target will begin this transition as a defect propagates to the target centre creating a one-arm spiral. Moving away from onset additional defects enter the spiral resulting in more arms at the centre (as many as six-arm spirals are observed in experiments). The spiral core will begin to move off centre [22] and the number of defects will increase. Eventually, the spiral core will annihilate with the sidewalls and again spiral defect chaos will form. Lastly, regular hexagons break down to bistable domains of stripes and hexagons relatively close to onset. The stripes will then fill the pattern and the transition to spiral defect chaos proceeds as it does for the case of parallel stripes at onset. Each of these onset planforms and transitions to spiral defect chaos are qualitatively similar to those reported for Rayleigh–Bénard convection. Further into the harmonic parameter range, spiral defect chaos breaks down as clumps of islands and stripes form throughout the experiment (see figure 8(d) in [22]). Qualitatively similar harmonic patterns to those described also occur in experiments using square lateral sidewalls. As expected [23] this includes a bulk phenomenon like spiral defect chaos (figure 2(f)).

At subharmonic onset, temporal inversion symmetry rules out the formation of hexagons and correspondingly only striped patterns are found. In most cases, parallel stripes emerge (figure 2(*g*)), although significant sidewall forcing can result in spirals (figure 2(*h*)). Near onset, dislocations and giant convex disclinations (see figure 2(*i*)) are commonly found. Moving away from onset more point defects in the forms of dislocations and disclinations enter the subharmonic patterns until the abrupt emergence of transverse modulations (figure 2(*j*)) that propagate from the sidewalls down the length of the stripes. Two as well as three sidewall foci [22] are common in transverse modulated stripes. Continuing through the region of transverse modulations (figure 3(*a*)) the base stripe pattern gradually breaks down as radial stripes form (figure 2(*k*)). Eventually, the radial stripes undergo instability and all discernible structure is lost to plumes that form throughout the experiment. With square sidewalls parallel stripes (figure 2(*l*)) are commonly observed both near and away from primary onset.

3. Coexistence and complex order

Coexisting harmonic and subharmonic modes interact to form several novel patterns in the coexistence parameter range. Coexistence patterns are found over a wide parameter range bounded by harmonic and subharmonic linear stability curves (figure 3) for conduction. Generally, these patterns can be divided into three broad classes: harmonic dominated, subharmonic dominated, and those with relatively equal power spectrum contributions from both temporal responses (figure 4). Harmonic dominated coexistence occurs near the harmonic parameter region; to the left of the bicritical point in figure 3(*a*). Moving from harmonic patterns into coexistence, subharmonics do not emerge as soon as the subharmonic marginal stability curve is crossed, rather coexistence is delayed until well into the parameter region as shown in figure 3(*b*) [18, 19, 24]. Initial subharmonic formations are localized as stripes pinned perpendicular to the sidewalls or forming as patches about defects in the harmonic pattern [18, 19]. Moving further into the coexistence region subharmonic stripes begin to form perpendicular to the base harmonic stripes (figure 4(*a*)). The harmonic component in these patterns contributes more than 60% of the pattern's total spectral power at an average wavenumber q^H approximately the same as that of nearby purely harmonic states. The subharmonic contribution to the patterns grows slowly over this parameter region and is at an average wavenumber q^S that is larger than that of purely subharmonic patterns [18, 22].

Subharmonic dominated coexistence occurs near the subharmonic parameter region (figure 3). In contrast to the previously described harmonic-coexistence boundary, harmonics emerge in the immediate vicinity of the harmonic marginal stability curve and are found to be present throughout the subharmonic base state (figure 4(*b*)). In our experiments the boundary, shown in figure 3(*b*), could only be reliably determined for $R < 5500$. For larger R the subharmonic patterns possessed transverse modulations whose wavenumbers are approximately q^H, causing reliable detection of the transition to not be possible using the spectral techniques we employed. The emerging harmonic component typically forms parallel stripes containing several domains of different orientations. With the emergence of a harmonic component q^S gradually increases from its value at the transition to coexistence. At this subharmonic-coexistence boundary q^H is again similar to the values displayed by purely harmonic and coexistence patterns near the harmonic-coexistence boundary. Moving further into the coexistence region, q^H steadily decreases.

Sufficiently far into the coexistence parameter region spectral power contributions from harmonic and subharmonic patterns abruptly become relatively equal and complex-ordered patterns form. A few well-defined wave vectors will begin to dominate the power spectrum q^H

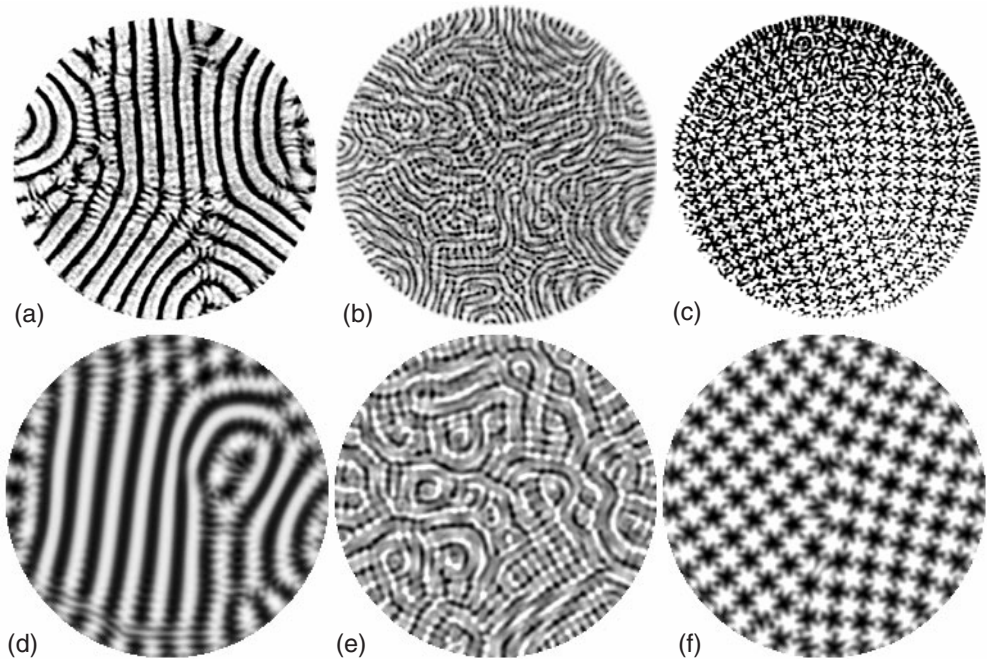

Figure 4. Comparison between representative coexisting patterns at $Pr = 0.93$ observed in experiments ((*a*)–(*c*)) and simulations ((*d*)–(*f*)). Harmonic dominated coexistence (*a*) at $R = 6679$, $\delta Fr = 3.50 \times 10^{-4}$, and $\omega = 97.9$. Subharmonic dominated coexistence (*b*) at $R = 6660$, $\delta Fr = 3.76 \times 10^{-4}$, and $\omega = 97.9$. Square quasiperiodic crystal (*c*) displaying domains with different orientations at $R = 6560$, $\delta Fr = 3.55 \times 10^{-4}$, and $\omega = 98.1$. Harmonic dominated coexistence (*d*) at $R = 6600$, $\delta Fr = 3.54 \times 10^{-4}$, and $\omega = 98.0$. Subharmonic dominated coexistence (*e*) at $R = 6800$, $\delta Fr = 4.061 \times 10^{-4}$, and $\omega = 98.0$. Square quasiperiodic crystal displaying two orientation domains (*f*) at $R = 6600$, $\delta Fr = 3.748 \times 10^{-4}$, and $\omega = 98.0$.

reaches its minimum value while q^S attains its maximum [19]. Initially these patterns display domains of ordered structures with various orientations (figure 4(*c*)). Near the formation of complex order (figure 3(*b*)) the domains continually change as defects emerge and annihilate, altering the domain orientations. All the experimental patterns described in these transitions are reproduced in our simulations of the Boussinesq equations; examples at similar parameter values to the experimental patterns are shown in figures 4(*d*)–(*f*).

Moving further into the parameter region of complex order (figure 3(*b*)) and away from the transition boundary the ordered domains coalesce into a single domain. As expected in this laterally isotropic system the single domain displays no preferred orientation. An example of a *square superlattice* found in simulations with periodic boundary conditions is shown in figure 5(*a*)[4]. This pattern is a superlattice since the harmonic and subharmonic spectral modes only require two indexing vectors to map out the dominant modes (i.e. the pattern could be placed on a torus in such a way that it would be cyclic). In fact, this square superlattice is periodic against translations by two lattice sites in the square (harmonic) sublattice. Qualitatively similar patterns which require more than two spectral indexing vectors are observed in experiments (figure 5(*b*)), we refer to these patterns as *square quasiperiodic crystals*[5]. Experiments find only quasiperiodic crystals in patterns of this type and we have

[4] An MPEG movie is available from stacks.iop.org/Non/16/C1.
[5] An AVI movie is available from stacks.iop.org/Non/16/C1.

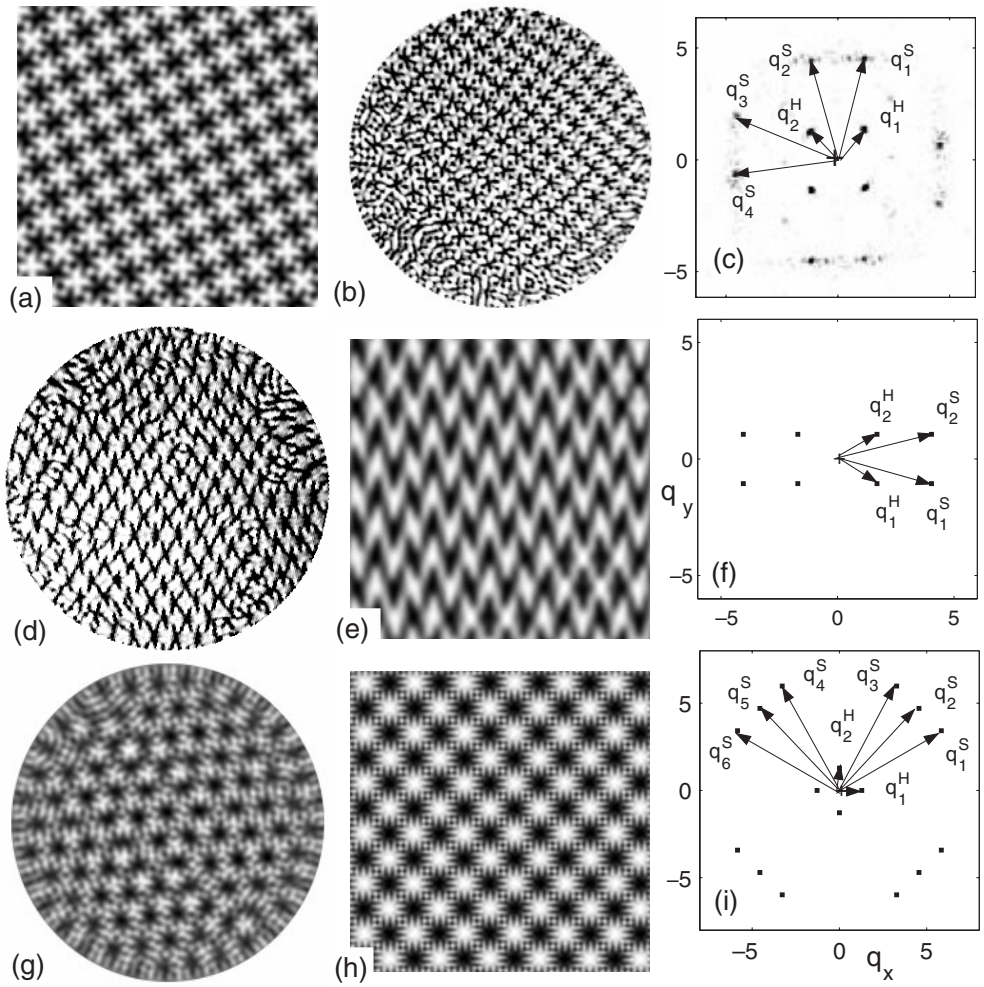

Figure 5. Complex-ordered patterns observed at $Pr = 0.930$ result from four-wave resonances between harmonic and subharmonic spectral modes. Square superlattice (*simulation*) (*a*) at $R = 4750$, $\delta Fr = 3.75 \times 10^{-4}$, and $\omega = 98.0$. Experiments find a square quasiperiodic crystal (*b*) at $R = 7030$, $\delta Fr = 3.88 \times 10^{-4}$, and $\omega = 95.3$. Both patterns display qualitatively similar spectral structure composed of four harmonic and eight subharmonic modes (*c*). Rhombic quasiperiodic crystal (*experiment*) (*d*) observed at $R = 5180$, $\delta Fr = 8.92 \times 10^{-4}$, and $\omega = 50.4$. Qualitatively similar patterns found in simulations (*e*) at $R = 3800$, $\delta Fr = 16.74 \times 10^{-4}$, and $\omega = 33$ with a characteristic spectral structure (*f*) composed of four harmonic and four subharmonic modes. Weakly violating spatial inversion symmetry of the layer about the midplane produces a (*g*) hexagonal quasiperiodic crystal (*simulation*) at $R = 4750$, $\delta Fr = 3.75 \times 10^{-4}$, and $\omega = 98.0$. Note that (*a*) and (*g*) form at the same parameter values; (*a*) if Boussinesq symmetry is imposed and (*g*) if it is violated. Another form of the (*h*) square quasiperiodic crystal (*simulation*) is found at $R = 7800$, $\delta Fr = 1.167 \times 10^{-4}$, and $\omega = 300$, in this case displaying 4 harmonic modes and 12 subharmonic modes (*i*).

not investigated if the existence of superlattices in the experiment is prevented by finite size effects from the lateral sidewalls.

Pattern and spectral structures in the vicinity of the complex order transition help reveal the mechanism producing these states. Unlike the majority of previously

reported complex-ordered patterns that result from three-wave resonances, all the observed quasiperiodic crystals and superlattices in this system rely on qualitatively different four-wave resonances (*resonant tetrads*) to form. These resonant tetrads always involve two harmonic and two subharmonic modes (figures 5(c), (f), (i)). Just prior to the formation of complex order, away from the bicritical point, coexistence patterns are quite complicated and display substantial disorder. Power spectra for these patterns possess two evenly populated rings, one at each wavenumber. As the transition to complex order begins, power in these q rings is drawn into sets of spectral modes satisfying well-defined resonant tetrads. These conditions as well as definitions for quasiperiodic crystals and superlattices in this system are presented in [19]. Patterns present after this transition, while still complex, are considerably more ordered. Our experiments and simulations are in quantitative agreement for the boundaries of complex-ordered patterns when $R \geqslant 6280$.

While Boussinesq simulations find that complex-ordered patterns bifurcate supercritically from both conduction and singly resonant patterns near the bicritical point [18], experiments find complicated coexistence patterns containing hexagons in the harmonic sublattice. Increasing R to move away from bicriticality simulations find complex order, including additional patterns [18, 19], over a widening range of δFr [24] up to $R \approx 6280$, where this parameter range agrees with experiments (figure 3(b)). In contrast, experimental patterns [19, 21] over this range contain fewer hexagons in the harmonic component with increasing R, but are unable to form complex-ordered states. Simulations that account for weak violations of Boussinesq symmetry find quasiperiodic crystals with a hexagonal harmonic component (figure 5(g)).

A variety of other complex-ordered patterns [18,19][6] exist at ω values away from $\omega \approx 100$ (figures 5(d), (e), and (h)), in part, because q^S is strongly dependent on ω. In addition to the examples shown in figure 5, other patterns have been reported [18, 19] for the cases of both different ω values as well as $-R$ values. Negative Rayleigh numbers ($-R$) correspond to physically heating from above, where $q^H > q^S$. We did not perform any experiments for these cases. All the quasiperiodic crystals and superlattices observed in experiments and simulations satisfy appropriate resonant tetrad conditions.

4. Conclusion

In conclusion we have used simulations and the first experiments of vertically oscillated convection to confirm linear stability predictions and investigate the patterns that form in the nonlinear parameter region. Experiments with significant dynamical range require thin layers with the appropriate physical characteristics and were not feasible prior to the development of the compressed gas convection apparatus. We find that singly resonant harmonic patterns display many of the characteristics of Rayleigh–Bénard convection, including the wavenumber being strongly dependent on geometry (d). In contrast, singly resonant subharmonic patterns display a wavenumber that is strongly dependent on ω as well as a time dependence that is characteristic of parametrically driven systems. In this sense, vertically oscillated convection is a composite of two well-studied pattern formation systems: Rayleigh–Bénard convection and Faraday waves. Over a wide parameter range we find that harmonic and subharmonic patterns are bistable. A number of novel coexistence patterns as well as the first examples of quasiperiodic crystals and superlattices in convection were reported. Resonant four-wave interactions between the temporal responses are found to be the formation mechanism of the quasiperiodic crystals and superlattices. After our initial report [24] of four-wave resonances

[6] An MPEG movie is available from stacks.iop.org/Non/16/C1.

producing complex order, resonant tetrads were also reported in Faraday experiments [12]. However, the majority of reported complex-ordered patterns rely on qualitatively different three-wave resonances. Our results suggest that there are a number of interesting patterns and transitions accessible in vertically oscillated convection. We have focused primarily on only one combination of Pr and ω and our initial trials at other values suggest that many interesting questions remain to be addressed in this system.

References

[1] Bénard H 1900 *Ann. Chim. Phys.* **7** 62–144
[2] Cross M C and Hohenberg P C 1993 *Rev. Mod. Phys.* **65** 851–1112
[3] Faraday M 1831 *Phil. Trans. R. Soc.* **52** 319–40
[4] Coullet P, Frisch T and Sonnino G 1994 *Phys. Rev.* E **49** 2087–90
[5] Residori S, Ramazza P L, Pampaloni E, Boccaletti S and Arecchi F T 1996 *Phys. Rev. Lett.* **76** 1063–6
[6] Pismen L M and Rubinstein B Y 1999 *Chaos, Solitons, and Frac.* **10** 761–76
[7] Lifshitz R 1997 *Rev. Mod. Phys.* **69** 1181–218
[8] Edwards W S and Fauve S 1993 *Phys. Rev.* E **47** R788–91
[9] Kudrolli A, Pier B and Gollub J P 1998 *Physica* D **123D** 99–111
[10] Arbell H and Fineberg J 1998 *Phys. Rev. Lett.* **81** 4384–7
[11] Arbell H and Fineberg J 2000 *Phys. Rev. Lett.* **84** 654–7
[12] Arbell H and Fineberg J 2002 *Phys. Rev.* E **65** 036224/1-27
[13] Pi H, Park S, Lee J and Lee K J 2000 *Phys. Rev. Lett.* **84** 5316–19
[14] Pampaloni E, Residori S, Soria S and Arecchi F T 1997 **78** 1042–5
[15] Herrero R, Große Westhoff E, Aumann A, Ackermann T, Logvin Y A and Lange W 1999 *Phys. Rev. Lett.* **82** 4627–30
[16] Gresho P M and Sani R L 1970 *J. Fluid Mech.* **40** 783–806
[17] Clever R, Schubert G, and Busse F H 1993 *J. Fluid Mech.* **253** 663–80
[18] Rogers J L 2001 *PhD thesis* Georgia Institute of Technology
Brausch O 2001 *PhD thesis* Bayreuth University
[19] Rogers J L, Pesch W, Brausch O and Schatz M F (in preparation)
[20] Pesch W 1996 *Chaos* **6** 348–57
[21] Rogers J L, Schatz M F, Bougie J L and Swift J B 2000 *Phys. Rev. Lett.* **84** 87
[22] Rogers J L, Schatz M F, Pesch W and Brausch O 2002 *New Directions in Statistical Physics—Applications in Econophysics, Bioinformatics, and Pattern Recognition* ed L T Wille (Berlin: Springer) to appear
[23] Bodenschatz E, Pesch W and Ahlers G 2000 *Ann. Rev. Fluid Mech.* **32** 709–78
[24] Rogers J L, Schatz M F, Brausch O and Pesch W 2000 *Phys. Rev. Lett.* **85** 4281